




Neuronal synchrony abnormalities associated with subclinical epileptiform activity in early-onset Alzheimer's disease

 Kamalini G. Ranasinghe,¹ Kiwamu Kudo,^{2,3} Leighton Hinkley,² Alexander Beagle,¹ Hannah Lerner,¹ Danielle Mizuiri,² Anne Findlay,² Bruce L. Miller,¹ Joel H. Kramer,¹ Maria Luisa Gorno-Tempini,¹ Gil D. Rabinovici,^{1,4} Katherine P. Rankin,¹ Paul A. Garcia,⁴ Heidi E. Kirsch,^{2,4} Keith Vessel^{1,5,†} and Srikantan S. Nagarajan^{2,†}

[†]These authors contributed equally to this work.

See Lam and Shafi (<https://doi.org/10.1093/brain/awac033>) for a scientific commentary on this article.

Since the first demonstrations of network hyperexcitability in scientific models of Alzheimer's disease, a growing body of clinical studies have identified subclinical epileptiform activity and associated cognitive decline in patients with Alzheimer's disease. An obvious problem presented in these studies is lack of sensitive measures to detect and quantify network hyperexcitability in human subjects. In this study we examined whether altered neuronal synchrony can be a surrogate marker to quantify network hyperexcitability in patients with Alzheimer's disease. Using magnetoencephalography (MEG) at rest, we studied 30 Alzheimer's disease patients without subclinical epileptiform activity, 20 Alzheimer's disease patients with subclinical epileptiform activity and 35 age-matched controls. Presence of subclinical epileptiform activity was assessed in patients with Alzheimer's disease by long-term video-EEG and a 1-h resting MEG with simultaneous EEG. Using the resting-state source-space reconstructed MEG signal, in patients and controls we computed the global imaginary coherence in alpha (8–12 Hz) and delta–theta (2–8 Hz) oscillatory frequencies. We found that Alzheimer's disease patients with subclinical epileptiform activity have greater reductions in alpha imaginary coherence and greater enhancements in delta–theta imaginary coherence than Alzheimer's disease patients without subclinical epileptiform activity, and that these changes can distinguish between Alzheimer's disease patients with subclinical epileptiform activity and Alzheimer's disease patients without subclinical epileptiform activity with high accuracy. Finally, a principal component regression analysis showed that the variance of frequency-specific neuronal synchrony predicts longitudinal changes in Mini-Mental State Examination in patients and controls. Our results demonstrate that quantitative neurophysiological measures are sensitive biomarkers of network hyperexcitability and can be used to improve diagnosis and to select appropriate patients for the right therapy in the next-generation clinical trials. The current results provide an integrative framework for investigating network hyperexcitability and network dysfunction together with cognitive and clinical correlates in patients with Alzheimer's disease.

- 1 Memory and Aging Center, Department of Neurology, University of California San Francisco, San Francisco, CA, USA
- 2 Department of Radiology and Biomedical Imaging, University of California San Francisco, San Francisco, CA, USA
- 3 Medical Imaging Business Center, Ricoh Company, Ltd, Kanazawa 920-0177, Japan
- 4 Epilepsy Center, Department of Neurology, University of California San Francisco, San Francisco, CA, USA
- 5 Mary S. Easton Center for Alzheimer's Disease Research, Department of Neurology, David Geffen School of Medicine, University of California Los Angeles, Los Angeles, CA 90095, USA

Correspondence to: Kamalini G. Ranasinghe
Memory and Aging Center, Department of Neurology
University of California San Francisco
675 Nelson Rising Lane, Suite 190, San Francisco
CA 94158-1207, USA
E-mail: kamalini.ranasinghe@ucsf.edu

Keywords: network hyperexcitability; epileptiform activity in Alzheimer's disease; magnetoencephalography; neuronal synchrony; imaginary coherence

Abbreviations: AD-EPI+ = Alzheimer's disease patients with subclinical epileptiform activity; AD-EPI- = Alzheimer's disease patients without subclinical epileptiform activity; CDR = Clinical Dementia Rating; LTM-EEG = long-term electroencephalography monitoring; lvPPA = logopenic variant of primary progressive aphasia; MCI = mild cognitive impairment; MEG = magnetoencephalography; M/EEG = magnetoencephalography with simultaneous EEG; MMSE = Mini-Mental State Examination

Introduction

Epileptic abnormalities in patients with Alzheimer's disease have been reported since the first accounts of Alzheimer's disease by Alois Alzheimer over a century ago.¹ The demonstration of network hyperexcitability in transgenic Alzheimer's disease mice² revived this largely overlooked phenomenon, and since then a growing body of clinical studies have identified subclinical epileptiform activity in cortical and hippocampal circuits in patients with Alzheimer's disease.^{3–8} These studies indicate that epileptiform abnormalities manifest early in the disease course, often precede the onset of cognitive decline and are associated with the genetic risk of Alzheimer's disease.^{9,10} Concurrently, numerous physiological studies have established potential mechanisms related to network hyperexcitability suggesting a vicious cycle where Alzheimer's disease proteinopathy—amyloid- β and tau—contributes to epileptogenesis,^{11–15} which in turn augments the aggregation and spread of disease proteins.^{16,17} The perspective of epileptic activity in Alzheimer's disease has since transformed from a secondary process of neurodegeneration to that of a modifiable contributor to disease pathology.¹⁸

While network hyperexcitability poses a core mechanism of Alzheimer's disease pathogenesis, epileptiform discharges which represent sporadic paroxysmal abnormalities of network activity are only detected in select patients in clinical assessments. Development of novel therapeutics that target network hyperexcitability, however, demands precise deciphering of neuronal circuit dysfunction in patients. The ubiquitous rhythmic oscillations in the brain that are altered by Alzheimer's disease pathology^{19–23} are reliable quantitative measures of network dysfunction. The degree to which abnormal oscillatory signatures can act as surrogate markers of network dysfunction associated with subclinical epileptiform activity has not been investigated in patients with Alzheimer's disease.

Here we tested the hypothesis that Alzheimer's disease patients with subclinical epileptiform activity (AD-EPI+) have more severely impacted network synchrony than Alzheimer's disease patients without subclinical epileptiform activity (AD-EPI-). We prospectively characterized patients into two subgroups as AD-EPI+ and AD-EPI- using two forms of sensitive neurophysiological monitoring: extended/long-term electroencephalography (LTM-EEG) and magnetoencephalography with simultaneous EEG (M/EEG). We leveraged the high spatial and precise temporal resolution of MEG to quantify network abnormalities based on long-range neuronal synchrony within specific oscillatory

frequencies of delta–theta (2–8 Hz) and alpha (8–12 Hz) in AD-EPI+ versus AD-EPI- patients.

Materials and methods

Subjects

Fifty patients with Alzheimer's disease (age, 60 ± 8) and 35 age-matched control subjects (age, 64 ± 6) were included in the study (Table 1). All patients with Alzheimer's disease met the National Institute of Aging–Alzheimer's Association criteria for probable Alzheimer's disease or mild cognitive impairment (MCI) due to Alzheimer's disease,^{24–26} and had CSF or amyloid-PET biomarkers supportive of an Alzheimer's disease diagnosis or subsequent histopathological confirmation at autopsy (Supplementary Table 1). Twenty Alzheimer's disease patients (40%) were identified as positive for subclinical epileptiform activity (AD-EPI+) based on LTM-EEG and M/EEG evaluations. Twenty-seven of the 50 patients (54%) included in the current study also took part in our previous observational study where we reported the incidence of subclinical epileptiform activity in Alzheimer's disease.⁴ All participants were recruited from research cohorts at the University of California San Francisco (UCSF) Memory and Aging Center. Clinical diagnosis for patients with Alzheimer's disease was established by consensus at a multidisciplinary team and confirmed with positive Alzheimer's disease biomarkers (Supplementary Table 1). Each Alzheimer's disease patient was further assigned to their specific Alzheimer's disease neurobehavioural phenotype. Specifically, we identified patients who met the diagnostic criteria for logopenic variant of primary progressive aphasia (lvPPA)²⁷ and posterior cortical atrophy²⁸ as atypical Alzheimer's disease phenotypes (lvPPA, $n=7$; posterior cortical atrophy, $n=11$). Age-matched normal controls were recruited from the community and the eligibility criteria included normal cognitive performance, normal MRI and absence of neurological, psychiatric or other major medical illnesses. Informed consent was obtained from all participants or their assigned surrogate decision makers. The study was approved by the UCSF Institutional Review Board.

Neurophysiological assessments to detect subclinical epileptiform activity

All patients underwent overnight long-term monitoring by video EEG (LTM-EEG) telemetry, followed by 1-h resting-state MEG

exam with simultaneous 21-lead EEG (M/EEG) the following day. Based on LTM-EEG and M/EEG recordings patients were identified as epileptiform-positive (AD-EPI+) and -negative (AD-EPI-).

LTM-EEG telemetry

Patients were evaluated at the Clinical and Translational Science Institute Clinical Research Center at Moffitt Hospital at UCSF. Monitoring included overnight long-term recording using silver cup electrodes in the standard international 10–20 electrode array, with 3 min of hyperventilation.

M/EEG

One-hour resting-state M/EEG was performed at the UCSF Biomagnetic Imaging Laboratory. The MEG was recorded with a whole-head MEG system (CTF) comprising 275 axial gradiometers (sampling rate = 600 Hz). Fiducial coils were placed at the nasion and left and right pre-auricular points to locate head position relative to the sensor array and later used to co-register MEG data with the brain MRI. During recordings, participants stayed supine, eyes closed and were encouraged to fall asleep. During the final 10 min the participants hyperventilated for 3 min and breathed normally for 7 min.

LTM-EEG and M/EEG were read by experienced epileptologists (P.A.G. and H.E.K.) and clinical neurophysiologists (K.G.R. and K.V.). The Spike Density Calculation Engine in Persyst-11 EEG software was used to help detect epileptiform activity on the LTM-EEG. Epileptiform activity on LTM-EEG or M/EEG was defined using the same criteria mentioned in our previous study⁴ and included the presence of a spike or sharp wave that fulfilled the specific criteria to be identified as an interictal epileptiform discharge (i.e. abrupt change in polarity with specific morphological spike and sharp wave characteristics that is clearly distinguished from background activity, a clear physiologic field, disrupted background, associated with subsequent slowing, or embedded in bursts of focal slowing).^{29,30} Normal EEG variants such as small sharp spikes and wicket spikes were not included as subclinical epileptiform activity. Entire recordings were reviewed by visual inspection, and determination of epileptiform activity was made by consensus between the clinicians who reviewed the recordings (P.A.G., H.E.K., K.G.R. and K.V. for LTM-EEG; H.E.K. and K.G.R. for M/EEG). Seventeen controls were monitored with both LTM-EEG and 1-h M/EEG (the same protocol as for patients with Alzheimer's disease). An additional eight controls were monitored with 1-h M/EEG. LTM-EEG and M/EEG recordings from controls were reviewed by the same team of clinicians as described above and were marked down as negative for epileptiform activity with consensus agreement. Ten control participants were only assessed via a 10-min resting MEG.

Neurophysiological assessment to quantify long-range neuronal synchrony

We estimated long-range synchrony using the source space reconstructed MEG data, for each subject, within frequency bands of alpha (8–12 Hz) and delta–theta (2–8 Hz).^{23,31} Neuronal synchrony measures were based on a 60-second continuous segment of resting state MEG recording. The analytic epochs for the patients with Alzheimer's disease were selected from the initial 10-min segment of the 1-h resting M/EEG recordings collected under the clinical protocol described above. The 60-s analytic epochs for the age-matched controls also came from the initial segments of the resting MEG recording sessions. The resting MEG data collection

protocols (for patients and controls) required the subject to be interactive with the examiner immediately before the data collection period and helped to achieve awake status data collection during the initial segment of the recordings. The spectral power density was examined in each subject's selected data epoch to reaffirm the characteristic spectral patterns of awake resting status of the participant. In addition, the simultaneous EEG collected from all Alzheimer's disease patients and some of the controls were also examined to confirm the awake resting status.

To estimate the long-range synchrony we computed voxelwise imaginary coherence using source-space reconstructed MEG data, for each subject, within frequency bands of alpha (8–12 Hz) and delta–theta (2–8 Hz).^{23,31} Imaginary coherence captures only the coherence that cannot be explained by volume spread and is a reliable metric for resting state functional connectivity analyses.³² Artefact detection was confirmed by visual inspection of sensor data and channels with excessive noise within individual subjects were removed prior to analysis. Tomographic reconstructions of the MEG data were generated using a head model based on each participant's structural MRI. Spatiotemporal estimates of neural sources were generated using time–frequency analyses implemented in the Neurodynamic Utility Toolbox for MEG (NUTMEG; <http://nutmeg.berkeley.edu>).³³ Tomographic volume of source locations (voxels) were computed through an optimized adaptive spatial filter (10 mm lead field) that weights each location relative to the signal of the MEG sensors.^{34,35} The source-space reconstruction approach provided amplitude estimations at each voxel derived through the linear combination of spatial weighting matrix with the sensor data matrix. We computed voxelwise global imaginary coherence at each voxel as the average of the Fisher's Z-transformed imaginary coherence values between a given voxel (10 mm isotropic) and all other voxels in the brain, for each subject. To minimize spatial frequency noise in the beamformer volumes, average and variance maps for each individual frequency band were calculated and smoothed using a Gaussian kernel with a width of $20 \times 20 \times 20$ mm full-width-at-half-maximum.

Neuropsychological and functional assessment

Each participant was assessed via Mini-Mental State Examination (MMSE, with appropriate permission), a structured caregiver interview to document the Clinical Dementia Rating scale (CDR) and a standard battery of neuropsychological tests³⁶ ([Supplementary material](#)).

MRI

Structural brain images were acquired from all participants ([Supplementary material](#)) and were used to generate individualized head models for source-space reconstruction of MEG sensor data.

Statistical analyses

Statistical comparisons for imaginary coherence analyses

We examined the group-level statistics in imaginary coherence in patients with Alzheimer's disease and age-matched control subjects, using statistical non-parametric whole-brain mapping methods incorporated in the NUTMEG toolbox.³³ Statistical significance was estimated by obtaining a permuted distribution (through $2N$ possible combinations of negations) and estimating the significance of the test statistic (imaginary

coherence) value from its position in this permuted distribution. To correct for multiple comparisons, we used 5% false discovery rate (FDR) in our analysis and thresholded the images with adjusted *P*-values. Specifically, we determined the corrected *P*-value threshold level at the 5% FDR cutoff level for all voxels that showed effects at the uncorrected $P < 0.01$ threshold. The voxels that survived the FDR correction were then further thresholded using cluster correction procedure in NUTMEG, with a cutoff level of 30 voxels (only the clusters with 30 congruent voxels remained), and *P*-values thresholded to $P < 0.01$. Clusters in the thresholded statistical maps were discarded if they fell below the 95% of null-distribution cutoff following permutation testing and did not meet the required minimum value of 30 contiguous voxels at $P < 0.01$. This approach minimized the possibility of observing spurious effects. The group contrasts were examined within each frequency band for the following contrasts: all Alzheimer's disease patients versus controls; AD-EPI+ versus controls; AD-EPI− versus controls.

To compare the network impacts from the Alzheimer's disease pathophysiological processes in AD-EPI+ versus AD-EPI−, we employed statistical mixed models. First, we extracted the voxelwise imaginary coherence values for each Alzheimer's disease patient, within the regions of interest that was identified as significantly different between all Alzheimer's disease patients and controls, for each frequency band (i.e. alpha and delta–theta). Next, we used the PROC MIXED procedure in SAS to build a mixed model, for each frequency band, and examined the pairwise group level difference between AD-EPI+ and AD-EPI− patients. The models incorporated a repeated measures design to incorporate multiple regions per subject and included region of interest label and subject identity as categorical information. Data from 173 and 583 voxels were included for alpha and delta–theta imaginary coherence models, respectively.

Logistic regression models and receiver operating characteristic curve analysis

We used a logistic regression model where the Alzheimer's disease subgroup identity (i.e. AD-EPI+, AD-EPI−) was the dependent variable and MEG-derived functional connectivity patterns were the predictor variables. We first defined the most affected voxel-level regions of interest in the contrast between all Alzheimer's disease versus controls, for alpha and delta–theta frequency bands. This selection was based on the *t*-statistic derived from the above contrast. To minimize regional dependency, we applied the additional criteria of >20 mm apart when selecting the voxel-level regions of interest. [Supplementary Table 2](#) lists the regional labels and Montreal Neurological Institute (MNI) coordinates of the selected regions of interest showing the greatest degree of alpha hyposynchrony and the greatest degree of delta–theta hypersynchrony. Next, we extracted the alpha and delta–theta imaginary coherence values for 10 regions of interest for each Alzheimer's disease patient. We then used a logistic regression-based discriminant analysis (PROC LOGISTIC in SAS) to quantify the extent of distinction between AD-EPI+ and AD-EPI− individuals based on imaginary coherence of alpha and delta–theta region of interest values. Specifically, we ran a series of models varying the number of predictor variables from two regions of interest (the top alpha region of interest and top delta–theta region of interest) to 10 regions of interest (top five alpha and top five delta–theta). The category identity of AD-EPI+ or AD-EPI− was the dependent variable of the models. Receiver operating characteristic (ROC) plots were constructed

to quantify the confidence limits and area-under-the curve (AUC) estimates for each model.

Assessment for regional associations between predominant epileptic zone and impaired neuronal synchrony

We also examined the regional associations between the regional patterns of impaired neuronal synchrony and the predominant epileptic zone, as the latter was localized to one of three hemispheric locations: frontal; temporal; parietal–occipital ([Supplementary material](#)).

Linear mixed models to examine rate of MMSE decline

We compared the rate of decline in MMSE AD-EPI+ and AD-EPI− patients using a linear mixed-effects model (SAS PROC MIXED). For this analysis we utilized all the multiple evaluations in our cohort including the retrospective assessments (with reference to their neurophysiological assessment), which included 88 total observations from 24 AD-EPI− patients and 68 total observations from 18 AD-EPI+ patients. Starting from each patient's first evaluation, we examined the longitudinal scores in MMSE. Patient identity was entered into the model as a repeated factor. Fixed effects were time from initial evaluation and the presence or absence of subclinical epileptiform activity. We also examined the same effects after incorporating age at MEG and education as covariates into the models.

Principal component regression analysis

We used a principal component regression approach to examine the associations between MMSE rate of decline and the imaginary coherence metrics. First, we calculated the MMSE slopes for each individual patient and control participant with multiple MMSE evaluations utilizing the retrospective data-points with reference to their neurophysiological assessment ($n=24$, $n=18$ and $n=29$, AD-EPI−, AD-EPI+ and controls, respectively). Next, we generated a data matrix including each subject's (row-vector) imaginary coherence values within the voxel-ROIs identified in the all Alzheimer's disease versus controls comparison, for alpha (173 columns) and delta–theta (583 columns) frequency bands. We used the first two principal components derived from a principal component analysis (PCA) of this data matrix as predictors in a multiple regression model to predict the MMSE slopes. Fit diagnostics for the multiple regression model based on Cook's *D* and DFITS measures identified a single observation consistently as an extreme outlier and we excluded this observation from our final regression model, thus including $n=24$, $n=17$ and $n=29$ subjects under AD-EPI−, AD-EPI+ and controls, respectively.

Statistical comparisons of demographic and clinical variables

For pairwise comparisons of continuous variables, *t*-tests were used for those that were normally distributed and Wilcoxon–Mann–Whitney tests for those that were not. For comparisons of proportions of categorical variables in contingency tables, Pearson chi-square (χ^2) tests were used when expected cell values were >5 and Fisher exact tests when they were <5. All statistical analyses were done using SAS software version 9.4 (SAS Institute Inc., Cary, NC).

Table 1 Participant demographics and clinical characteristics

Characteristic	Controls (n = 35)	AD-EPI– (n = 30)	AD-EPI+ (n = 20)	P*
Age, years	63.0 ± 5.8	60.7 ± 8.3	59.9 ± 6.7	0.122
Female sex, n (%)	22 (62.8)	17 (56.7)	12 (60.0)	0.879
White, n (%) ^a	25 (92.6)	27 (96.4)	19 (100.0)	0.449
Education, years	17.4 ± 1.6	15.7 ± 2.6	17.0 ± 2.7	0.012^b
Right handedness, n (%)	28 (80.0)	25 (83.3)	18 (90.0)	0.629
ApoE ε4 carrier, n (%)	4 (16.0)	12 (44.4)	9 (47.4)	0.043^b
MMSE ^c	29.6 ± 0.7	21.3 ± 5.8	21.5 ± 4.7	0.911
CDR ^d	0	1.0 (0.5–1.0)	1.0 (0.5–1.0)	0.351
CDR-SOB ^d	0	4.5 (3.5–5.0)	4.7 (3.3–6.5)	0.690
Age at disease onset, years	–	54.0 (50.0–58.0)	53.5 (50.0–57.5)	0.882
Disease duration	–	5.4 (4.7–7.2)	4.8 (3.8–6.5)	0.440
Early onset Alzheimer's disease, n (%)	–	28 (93.3)	19 (95.0)	0.44
Atypical Alzheimer's disease, n (%)	–	11 (36.7)	7 (35.0)	0.904
Generalized slowing on LTM-EEG, n (%)	–	7 (23.3)	6 (30.0)	0.598
Asymmetric/focal slowing on LTM-EEG, n (%)	–	4 (13.3)	3 (15.0)	0.868
Generalized slowing on M/EEG, n (%)	–	13 (43.3)	6 (30.0)	0.341
Asymmetric/focal slowing on M/EEG, n (%)	–	5 (16.7)	8 (40.0)	0.065
On AChE-I, n (%)	–	15 (50.0)	12 (60.0)	0.487
On memantine, n (%)	–	1 (3.3)	1 (5.0)	0.768
On AChE-I and memantine, n (%)	–	7 (23.3)	3 (15.0)	0.470
On antidepressants, n (%)	–	15 (50.0)	11 (55.0)	0.729

Values for age, education and MMSE are means ± standard deviation (SD). Values for CDR, CDR-SOB, age at disease onset and disease duration are medians with interquartile ranges in parentheses. AChE-I = acetylcholinesterase inhibitor; Alzheimer's disease = Alzheimer's disease; AD-EPI– = Alzheimer's disease patients without epileptiform activity; AD-EPI+ = Alzheimer's disease patients with epileptiform activity; ApoE = apolipoprotein E; CDR-SOB = CDR-Sum of Boxes.

*Statistical tests: P-values are reported from one-way ANOVA with pairwise comparisons for age and education, Pearson χ^2 test for sex and apolipoprotein-ε4 carrier, race and handedness, for the full cohort including the three groups. P-values are reported Pearson χ^2 test between AD-EPI+ and AD-EPI– for atypical Alzheimer's disease, generalized slowing on EEG, asymmetric/focal slowing on EEG, generalized slowing on MEG, asymmetric/focal slowing on MEG, usage of AChE-I, memantine, combined AChE-I and memantine and antidepressant use. P-values for early-onset Alzheimer's disease are reported from Fisher's exact test between AD-EPI+ and AD-EPI–. P-values for the MMSE is reported from unpaired t-test and for CDR, CDR-SOB, age at disease onset and disease duration are reported from Wilcoxon–Mann–Whitney test, comparing the two patient cohorts.

^aRace or ethnic group was self-reported. Two patients with Alzheimer's disease and eight controls opted out from reporting race.

^bPairwise comparison for education between controls and AD-EPI– showed a statistically significant difference ($P = 0.011$); pairwise analyses showed significant higher proportions of Apolipoprotein E ε4 carrier status in Alzheimer's disease compared to controls (16% versus 45% in controls and all Alzheimer's disease, $P = 0.0125$), but no differences between the two Alzheimer's disease cohorts ($P = 0.844$).

^cScores on the MMSE range from 0 to 30, with higher scores denoting better cognitive function.

^dScores on the CDR range from 0 to 3 and scores on the CDR-SOB range from 0 to 18, with higher scores denoting more disability.

Data availability

All data associated with this study are present in the paper or in the [Supplementary material](#). Anonymized subject data will be shared on request from qualified investigators for the purposes of replicating procedures and results, and for other non-commercial research purposes within the limits of participants' consent. Correspondence and material requests should be addressed to the corresponding author.

Results

Demographic and clinical characteristics

Both AD-EPI– and AD-EPI+ were mild-to-moderately impaired in dementia severity, and did not differ from each other in demographic, clinical and cognitive characteristics including age at onset, disease duration, fraction of early-onset Alzheimer's disease, fraction of atypical Alzheimer's disease, Apo-ε4 carrier status and use of medications (Table 1 and [Supplementary Table 3](#)). Consistent with our previous reports, AD-EPI+ patients showed a faster decline in MMSE and executive function than AD-EPI–, although there were no group differences in rate of change in memory, visuospatial and language abilities ([Supplementary Table 4](#)). Background activity characterized by generalized and

asymmetric/focal slowing was not different between AD-EPI+ versus AD-EPI– (Table 1). Epileptiform discharges in AD-EPI+ subjects were most often detected in temporal lobes ([Supplementary Fig. 1](#)).

AD-EPI+ have more severe neuronal synchrony abnormalities than AD-EPI– patients.

We quantified the neuronal synchrony within alpha (8–12 Hz) and delta–theta (2–8 Hz) frequency oscillations by estimating imaginary coherence (IC) in a voxelwise whole-brain analysis. Comparison of all Alzheimer's disease patients (i.e. the full cohort of Alzheimer's disease patients) versus age-matched controls demonstrated region-specific patterns of reduced alpha synchrony in the posterior parieto-temporal–occipital regions and increased delta–theta synchrony in the dorsal frontal and parietal cortices, consistent with previous reports²³ ([Supplementary Fig. 2](#)). AD-EPI+ patients showed notably enhanced regional reductions of alpha synchrony and increased regional patterns of delta–theta synchrony relative to AD-EPI– patients (Fig. 1). To quantify these distinctions, we compared each Alzheimer's disease subgroup with age-matched controls. AD-EPI+ patients versus controls showed greater reductions in alpha synchrony and larger increases in delta–theta synchrony than AD-EPI– patients versus controls (Fig. 2). Additional analyses demonstrated that comparable patterns of frequency-specific and region-dependent synchrony

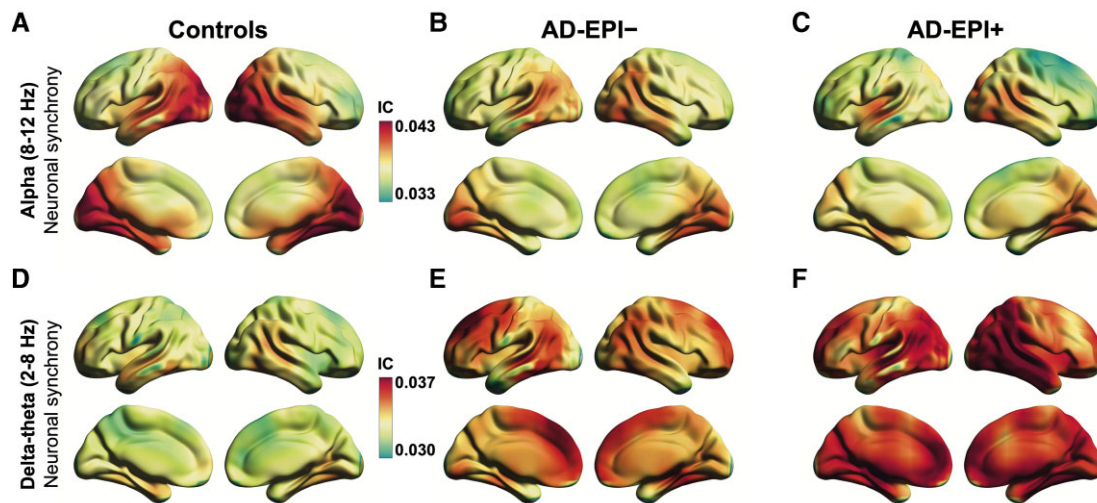


Figure 1 Frequency-specific neuronal synchrony abnormalities in Alzheimer's disease patients with and without epileptiform activity. (A–F) The strength of functional connectivity as global imaginary coherence (IC) within alpha (8–12 Hz) and delta–theta (2–8 Hz) frequency oscillation bands. Controls showed highest imaginary coherence within the alpha band (8–12 Hz) in occipitoparietal cortices (A). AD-EPI– and AD-EPI+ patients showed reduced imaginary coherence within the alpha band, where the latter group showed a greater degree of reductions (B and C). Within the delta–theta band, controls showed highest imaginary coherence in frontal and parietal cortices (D). AD-EPI– and AD-EPI+ both showed enhanced delta–theta imaginary coherence where the latter group showed greater degree of enhancement (E and F). The colour maps are thresholded with a cluster correction of 30 voxels ($P < 0.01$) and at 5% false discovery rate ($n = 30$, AD-EPI+; $n = 20$ AD-EPI–; $n = 35$ age-matched controls). Alzheimer's disease = Alzheimer's disease; AD-EPI– = Alzheimer's disease patients without epileptiform activity; AD-EPI+ = Alzheimer's disease patients with epileptiform activity; IC = imaginary coherence.

deficits are observed in AD-EPI+ patients when subtyped according to the modality by which the subclinical epileptiform activity was detected (i.e. via LTM-EEG or M/EEG; [Supplementary Fig. 3](#)). Next, we directly contrasted AD-EPI+ and AD-EPI– patients in a statistical linear mixed model using a region of interest approach. For this

analysis, we employed a mixed-effects model with repeated measures and included the statistically significant regions of interest from the contrast between all Alzheimer's disease versus controls as predictors. AD-EPI+ patients showed greater reductions in alpha synchrony in the parieto-temporal-occipital cortices

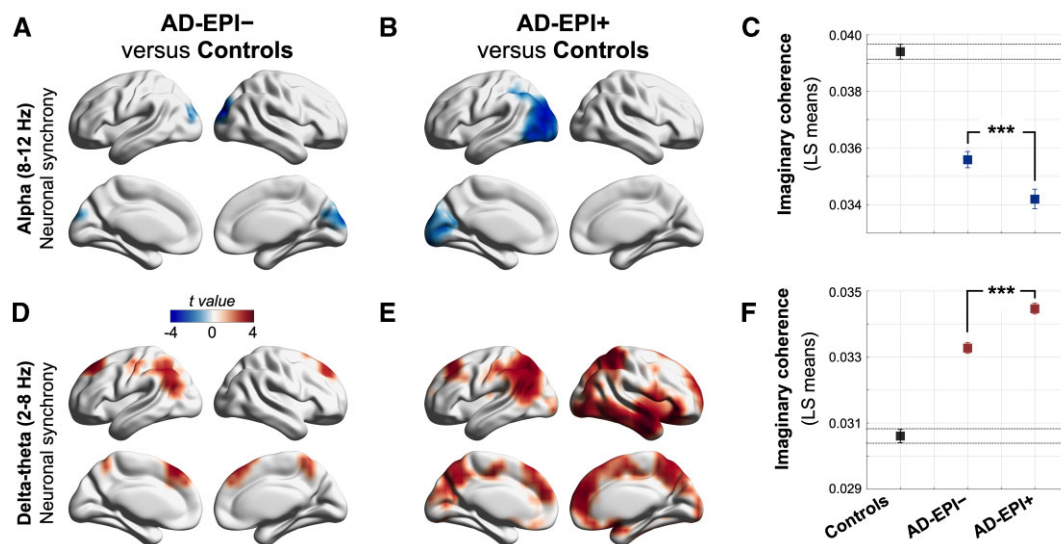


Figure 2 Distinctive regional patterns of neuronal synchrony deficits in Alzheimer's disease patients with and without epileptiform activity. (A–F) Statistical comparisons of imaginary coherence between groups. Within the alpha band, AD-EPI– and AD-EPI+ showed significantly reduced imaginary coherence compared to controls, over bilateral occipital cortices, with more extensive regional involvement in AD-EPI+ (A and B). Pairwise comparison showed AD-EPI+ with significantly lower alpha imaginary coherence than AD-EPI– (C). AD-EPI– and AD-EPI+ showed significantly increased delta–theta imaginary coherence compared to controls, over bilateral frontal and parietal cortices, with more extensive involvement in AD-EPI+ (D and E) and pairwise comparison showed AD-EPI+ with significantly higher delta–theta imaginary coherence than AD-EPI– (F). Each brain rendering depicts the t-maps from voxelwise comparison of global imaginary coherence between groups. The colour maps are thresholded with a cluster correction of 30 voxels ($P < 0.01$) and at 5% FDR. (C and F) depict least squares (LS)-means and 95% confidence-limits ($n = 30$, AD-EPI+; $n = 20$ AD-EPI–; $n = 35$ age-matched controls). Alzheimer's disease = Alzheimer's disease; AD-EPI– = Alzheimer's disease patients without epileptiform activity; AD-EPI+ = Alzheimer's disease patients with epileptiform activity; IC = imaginary coherence.

(Fig. 2C; $t = 6.05$, $P < 0.0001$) and greater enhancements in delta–theta synchrony in the dorsomedial frontal and parietal cortices (Fig. 2F; $t = -13.66$, $P < 0.0001$) than AD-EPI– patients.

A direct comparison of voxelwise alpha and delta–theta imaginary coherence between AD-EPI+ and AD-EPI– patients revealed additional regional differences between these two subgroups (Supplementary Fig. 4). For example, AD-EPI+ showed reduced alpha synchrony in the dorsal aspect of the central, parietal and temporal cortices and increased delta–theta synchrony in the bilateral posterior parietal and right temporal cortices compared to AD-EPI–. The directionality of these frequency-specific changes from the direct comparison were consistent with the results from each subgroup versus age-matched controls shown above. The regional significance of the frequency-specific deficits in AD-EPI+ versus AD-EPI– remains to be explored in future studies. We further examined whether there are regional associations between the predominant epileptiform zone in AD-EPI+ patients and the most affected voxel-level regions of interest in alpha hyposynchrony and delta–theta hypersynchrony. To this end we first identified the quartiles of AD-EPI+ patients with the largest deviations of alpha hyposynchrony and delta–theta hypersynchrony in each region of interest (Supplementary material). Next, we denoted the predominant epileptiform zone in these subjects to examine any specific spatial pattern (Supplementary Fig. 5 and Supplementary Table 5). This analysis revealed no specific regional relationships, a finding which indicated widespread network dysfunction in Alzheimer’s disease that extends beyond the regional boundaries of a sporadic subclinical epileptic abnormality.

Quantitative neuronal synchrony abnormalities can distinguish between AD-EPI+ from AD-EPI– patients

We used a logistic regression model and an ROC curve analysis to examine the potential of altered neuronal synchrony to discriminate between AD-EPI+ and AD-EPI– patients. The predictors of the logistic regression models included altered alpha and delta–theta synchrony (z-score) from the most impaired voxel-level regions of interest as defined in the contrast between all Alzheimer’s disease versus controls (Supplementary Table 2). We ran a series of

models varying the number of predictor regions of interest from two (i.e. the most affected alpha region of interest and the most affected delta–theta region of interest) to 10 (i.e. top five alpha regions of interest and top five delta–theta regions of interest). The most affected voxel-level regions of interest in alpha and delta–theta were the left inferior temporal cortex and right middle temporal cortex, respectively (Supplementary Table 5). We found that even with a single region of interest per frequency band, alpha hyposynchrony and delta–theta hypersynchrony have the capacity to distinguish AD-EPI+ patients from AD-EPI– with high accuracy denoted by an AUC of 0.73 (Fig. 3A; AUC 0.73; CI, 0.58–0.89; $\chi^2 = 8.73$, $P = 0.0031$). The accuracy of discrimination increased with increasing number of predictor regions of interest in the models, where it reached 0.82 with three and 0.87 with five predictor regions of interest per frequency band (Fig. 3A; three regions of interest: AUC 0.82; CI, 0.70–0.94; $\chi^2 = 27.48$, $P < 0.0001$; five regions of interest: AUC 0.87; CI, 0.78–0.97; $\chi^2 = 56.38$, $P < 0.0001$).

Neuronal synchrony was associated with the rate of change in MMSE

Previously, we showed that AD-EPI+ patients have a faster rate of decline in MMSE than AD-EPI– patients.⁴ To examine whether the variance in MMSE rate of decline can be explained by the variance of altered neuronal synchrony we used a PCA-correlation analysis. The first two PCA components derived from the concatenated alpha and delta–theta imaginary coherence matrices explained 47% of the MMSE variance in the combined cohort of patients and controls (Supplementary Fig. 6). A multiple regression model based on the first two PCA components significantly predicted the MMSE rate of decline (Fig. 3B), indicating a gradation of MMSE slopes where age-matched controls represented flat slopes while AD-EPI+ patients represented the steepest declines in MMSE.

Discussion

In this study, we demonstrate how quantitative neurophysiological indices can be used to detect a greater degree of network dysfunction in AD-EPI+ than AD-EPI– patients. An important deduction from our results is that frequency-specific neural synchronization

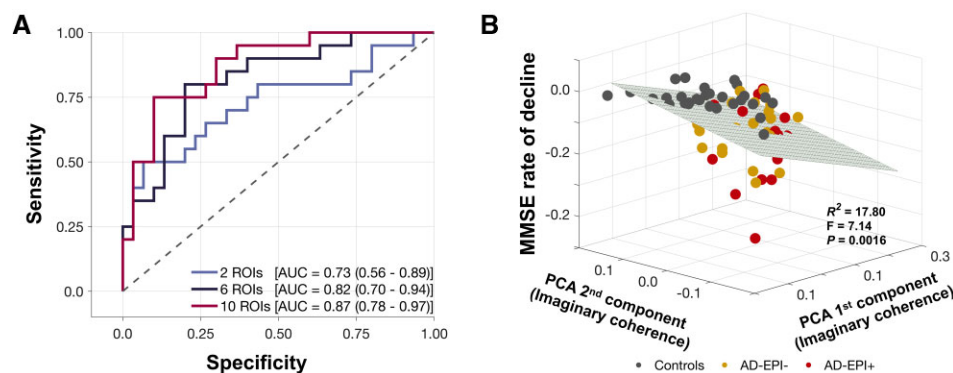


Figure 3 Neuronal synchrony indices distinguish between AD-EPI+ from AD-EPI– and are associated with rate of change in MMSE. (A) The ROC curves derived from logistic regression analyses for the discriminability between AD-EPI– and AD-EPI+ based on alpha and delta–theta imaginary coherence values from the most affected voxel-level regions of interest (varying from 1, 3, or 5 per frequency band). Longitudinal change in MMSE was significantly predicted by the first two principal components of the imaginary coherence matrix including alpha and delta–theta imaginary coherence in the full cohort (B). (A) $n = 30, 20, 35$, AD-EPI–, AD-EPI+ and controls; (B) $n = 17, 24, 29$, AD-EPI+, AD-EPI– and controls). Alzheimer’s disease = Alzheimer’s disease; AD-EPI– = Alzheimer’s disease patients without epileptiform activity; AD-EPI+ = Alzheimer’s disease patients with epileptiform activity; IC = imaginary coherence; MMSE = Mini Mental State Examination; ROC = receiver operating characteristic.

abnormalities which represent dimensional changes of network dysfunction in Alzheimer's disease are also sensitive to category boundaries defined along the degree of network hyperexcitability as EPI+ and EPI-. Although an increasing number of clinical studies have supported the hypothesis that network hyperexcitability could be a contributor to disease pathogenesis of Alzheimer's disease, epileptiform discharges in patients with Alzheimer's disease are still widely considered as a binary biomarker of hyperexcitability. Our findings challenge this view and demonstrate that both network dysfunction and network hyperexcitability exist on a closely coupled spectrum of severity in Alzheimer's disease. Indices of network dysfunction, as such, provide useful quantitative tools to probe network hyperexcitability in Alzheimer's disease. Emerging basic science evidence further supports the confluence of network dysfunction and network hyperexcitability in Alzheimer's disease pathophysiology. The current study provides an integrative framework to investigate network dysfunction and hyperexcitability and to quantify the network impact of Alzheimer's disease pathophysiology in a clinical population.

Comorbid and pathological associations of epileptic activity and Alzheimer's disease pathophysiology

Key findings from the current study strongly support the premise that epileptiform events represent integral manifestations of disease mechanisms in Alzheimer's disease. First, our finding that AD-EPI+ showing greater deficits in alpha synchrony bears important pathophysiological relevance in the context that alpha hypo-synchrony is regionally associated with high levels of pathological tau and related cognitive dysfunction in patients with Alzheimer's disease.^{23,37} Alpha oscillations are widely considered as inhibitory modulators of neuronal and network activity in the brain where higher alpha power and synchrony downregulate the irrelevant information while keeping a high signal-to-noise ratio of task-relevant information. It is therefore conceivable that reduced alpha oscillatory activity may contribute to network hyperexcitability as a downstream effect. Although neuronal hypoactivity is seemingly contradictory to a pro-epileptic phenotype, growing basic science evidence indicates that epileptic events represent a combination of heterogeneous aberrations at the level of single units including increases as well as decreases in firing across excitatory and inhibitory cell classes, and suggest potential mechanisms where glutamatergic abnormalities may give rise to network hyperexcitability.³⁸

Second, our study demonstrates that increased delta–theta oscillatory signature is higher in AD-EPI+ than AD-EPI- patients. Increased delta–theta oscillations in patients with Alzheimer's disease has been consistently linked to abnormal amyloid- β accumulation.^{23,37,39,40} In transgenic Alzheimer's disease mice network hyperexcitability and hyperactive neuronal states were reliably linked to toxic effects of amyloid- β and other metabolites of amyloid precursor protein (APP), suggesting that amyloid- β -mediated impaired GABAergic inhibitory transmission^{12,14} may contribute to network instability in the epileptic phenotype in Alzheimer's disease. Further support for comorbid pathophysiological processes of Alzheimer's disease and epileptiform activity comes from clinical trials using anti-seizure drugs in Alzheimer's disease. For example, the anti-epileptic agent levetiracetam stabilized the network abnormalities by reducing 1–4 Hz synchrony and enhancing 13–25 Hz synchrony in patients with Alzheimer's disease.⁴¹ A new clinical trial has shown that low-dose levetiracetam improves accuracy in

spatial memory and executive function in Alzheimer's disease patients with epileptiform activity.⁴² It has also been shown previously that levetiracetam suppresses hippocampal hyperactivity and improves hippocampal-dependent pattern separation ability in patients with MCI.⁴³ Therefore, electrophysiological indices that are sensitive to epileptic activity in Alzheimer's disease are not only surrogates of network hyperexcitability but also indicators of the full-scale functional consequences associated with Alzheimer's disease pathophysiology.

Neuronal synchrony deficits signify wider network-level abnormalities in Alzheimer's disease

Clinical studies have clearly demonstrated that pathological hyper-synchronous patterns of brain activity in patients with focal epilepsy extend beyond the region from which epileptiform discharges and seizures can be recorded.^{44–47} This is also consistent with the evolving undertraining of the pathogenesis of epilepsy as a phenomenon of network dysfunction where the traditional concept of an 'ictal network' has replaced the classic concept of 'epileptogenic zone'. In this context, our finding that regional patterns of neuronal synchrony deficits are spatially dissociated from the location of epileptiform abnormalities indicates that neuronal synchrony deficits signify network-level abnormalities above and beyond the localization of spikes and sharps. Furthermore, previous clinical studies reported a relatively higher occurrence of abnormal electrophysiological events during transition to and from sleep compared to awake brain states in patients with Alzheimer's disease. The high sensitivity of quantitative neuronal synchrony measures during awake to distinguish between AD-EPI+ and AD-EPI- indicates that manifestations of underlying network dysfunction spans across different 'brain states'. Future studies to better characterize the mechanisms by which epileptic activity interacts with the neural architecture in the human brain will be of great importance to advance our understanding of the network hyperexcitability in Alzheimer's disease.

Implications of quantitative indicators of epileptiform activity in Alzheimer's disease for clinical trials

The current results present important twofold implications for clinical trials in Alzheimer's disease. First, as network-stabilizing therapies hold promise to be disease-modifying agents, biomarkers sensitive to network hyperexcitability play a key role in detecting and quantifying network hyperexcitability to stratify candidates for the optimum intervention and to measure therapeutic success. The regional patterns of most affected anatomical areas within each frequency oscillation reported in the current study provide crucial information to be validated in independent larger cohorts to establish population statistics for network measures and establish biologically meaningful cutoffs for clinical trials. Second, the demonstration of network dysfunction and network hyperexcitability in a spectrum of severity associated with Alzheimer's disease pathophysiology signifies the importance of epileptic phenotype in Alzheimer's disease for clinical trials targeting amyloid- β - and tau-mediated pathogenic pathways. The results from this study raise the intriguing question regarding the nature and extent of the contribution of underlying network hyperexcitability to many failed clinical trials of amyloid- and tau-lowering approaches where this variable was largely ignored. With clinical trials pivoting towards earlier interventions,

quantifiable measures of network hyperexcitability are therefore attractive biomarkers for both network-stabilizing and protein-lowering therapeutic strategies.

Limitations

Our findings should be considered in the context of the following limitations. First, given the extended demand for time and resources for LTM-EEG our sample size was limited to 50 Alzheimer's disease patients, which restricted the ability to search for genetic, environmental and other factors associated with the quantitative surrogates of network hyperexcitability. Second, given the same high resource demand, LTM-EEG monitoring was not done for controls, and future studies on healthy ageing are needed to identify the effect of ageing on network hyperexcitability. Third, because the current Alzheimer's disease cohort is predominantly early-onset Alzheimer's disease phenotype future studies are needed to generalize the results to the more common late-onset Alzheimer's disease population.

Conclusions and future directions

In summary, we demonstrate quantitative and dimensional features of network dysfunction in patients with Alzheimer's disease that can distinguish the clinical expression of network hyperexcitability. Frequency-specific neuronal synchrony deficits may be important targets for network-stabilizing therapies with potential to delay or prevent the disease progression in Alzheimer's disease. Key topics for future studies are to investigate the longitudinal relationships between network dysfunction and hyperexcitability along the clinical course of Alzheimer's disease and to identify convergent quantitative electrophysiological signatures from EEG to develop into clinically viable network biomarkers.

Acknowledgements

We would like to thank all of the study participants and their families for their generous support to our research.

Funding

This study was supported by the National Institutes of Health grants: K08AG058749 (K.G.R.), F32AG050434-01A1 (K.G.R.), K23AG038357 (K.A.V.), P50-AG023501 (B.L.M. and G.D.R.); R01NS100440 (S.S.N.), R01DC017091 (S.S.N.), R01AG062196 (S.S.N.); a research contract with Ricoh MEG Inc. (S.S.N.); a grant from John Douglas French Alzheimer's Foundation (K.A.V.); grants from Larry L. Hillblom Foundation: 2015-A-034-FEL (K.G.R.) and 2019-A-013-SUP (K.G.R.); a grant from the Alzheimer's Association: (PCTRB-13-288476) (K.A.V.), and made possible by Part the CloudTM (ETAC-09-133596), and a gift from the S. D. Bechtel Jr. Foundation.

Competing interests

K.G.R., A.R., G.D.R., K.P.R., W.J.J., H.L., D.M., M.L.G., P.V., X.X., C.C., K.K., L.I., R.L.J., A.S. declare no competing interests relevant to this work. B.L.M. has the following disclosures: serves as Medical Director for the John Douglas French Foundation; Scientific Director for the Tau Consortium; Director/Medical Advisory Board of the Larry L. Hillblom Foundation; and Scientific Advisory Board

Member for the National Institute for Health Research Cambridge Biomedical Research Centre and its subunit, the Biomedical Research Unit in Dementia, UK. S.S.N. serves on the scientific advisory board for Rune Labs Inc.

Supplementary material

Supplementary material is available at *Brain* online.

References

1. Alzheimer A, Forstl H, Levy R. On certain peculiar diseases of old age. *Hist Psychiatry*. 1991;2(5 Pt 1):71–101.
2. Palop JJ, Chin J, Roberson ED, et al. Aberrant excitatory neuronal activity and compensatory remodeling of inhibitory hippocampal circuits in mouse models of Alzheimer's disease. *Neuron*. 2007;55(5):697–711.
3. Vossel KA, Beagle AJ, Rabinovici GD, et al. Seizures and epileptiform activity in the early stages of Alzheimer disease. *JAMA Neurol*. 2013;70(9):1158–1166.
4. Vossel KA, Ranasinghe KG, Beagle AJ, et al. Incidence and impact of subclinical epileptiform activity in Alzheimer's disease. *Ann Neurol*. 2016;80(6):858–870.
5. Lam AD, Deck G, Goldman A, Eskandar EN, Noebels J, Cole AJ. Silent hippocampal seizures and spikes identified by foramen ovale electrodes in Alzheimer's disease. *Nat Med*. 2017;23(6):678–680.
6. Horvath A, Szucs A, Hidasi Z, Csukly G, Barcs G, Kamondi A. Prevalence, semiology, and risk factors of epilepsy in Alzheimer's disease: An ambulatory EEG study. *J Alzheimers Dis*. 2018;63(3):1045–1054.
7. Lam AD, Sarkis RA, Pellerin KR, et al. Association of epileptiform abnormalities and seizures in Alzheimer disease. *Neurology*. 2020;95(16):e2259–e2270.
8. Horvath AA, Papp A, Zsuffa J, et al. Subclinical epileptiform activity accelerates the progression of Alzheimer's disease: A long-term EEG study. *Clin Neurophysiol*. 2021;132(8):1982–1989.
9. Voglein J, Noachtar S, McDade E, et al. Seizures as an early symptom of autosomal dominant Alzheimer's disease. *Neurobiol Aging*. 2019;76:18–23.
10. Ponomareva NV, Korovaitseva GI, Rogaev EI. EEG alterations in non-demented individuals related to apolipoprotein E genotype and to risk of Alzheimer disease. *Neurobiol Aging*. 2008;29(6):819–827.
11. Busche MA, Konnerth A. Impairments of neural circuit function in Alzheimer's disease. *Philos Trans R Soc Lond B Biol Sci*. 2016;371(1700):20150429.
12. Palop JJ, Mucke L. Network abnormalities and interneuron dysfunction in Alzheimer disease. *Nat Rev Neurosci*. 2016;17(12):777–792.
13. Busche MA, Chen X, Henning HA, et al. Critical role of soluble amyloid-beta for early hippocampal hyperactivity in a mouse model of Alzheimer's disease. *Proc Natl Acad Sci U S A*. 2012;109(22):8740–8745.
14. Verret L, Mann EO, Hang GB, et al. Inhibitory interneuron deficit links altered network activity and cognitive dysfunction in Alzheimer model. *Cell*. 2012;149(3):708–721.
15. Lei M, Xu H, Li Z, et al. Soluble Abeta oligomers impair hippocampal LTP by disrupting glutamatergic/GABAergic balance. *Neurobiol Dis*. 2016;85:111–121.
16. Wu JW, Hussaini SA, Bastille IM, et al. Neuronal activity enhances tau propagation and tau pathology in vivo. *Nat Neurosci*. 2016;19(8):1085–1092.

17. Bero AW, Yan P, Roh JH, et al. Neuronal activity regulates the regional vulnerability to amyloid-beta deposition. *Nat Neurosci.* 2011;14(6):750–756.
18. Styr B, Slutsky I. Imbalance between firing homeostasis and synaptic plasticity drives early-phase Alzheimer's disease. *Nat Neurosci.* 2018;21(4):463–473.
19. Babiloni C, Del Percio C, Lizio R, et al. Abnormalities of cortical neural synchronization mechanisms in patients with dementia due to Alzheimer's and Lewy body diseases: An EEG study. *Neurobiol Aging.* 2017;55:143–158.
20. Nakamura A, Cuesta P, Kato T, et al. Early functional network alterations in asymptomatic elders at risk for Alzheimer's disease. *Sci Rep.* 2017;7(1):6517.
21. de Haan W, Stam CJ, Jones BF, Zuiderwijk IM, van Dijk BW, Scheltens P. Resting-state oscillatory brain dynamics in Alzheimer disease. *J Clin Neurophysiol.* 2008;25(4):187–193.
22. Osipova D, Ahveninen J, Jensen O, Ylikoski A, Pekkonen E. Altered generation of spontaneous oscillations in Alzheimer's disease. *NeuroImage.* 2005;27(4):835–841.
23. Ranasinghe KG, Cha J, Iaccarino L, et al. Neurophysiological signatures in Alzheimer's disease are distinctly associated with TAU, amyloid-beta accumulation, and cognitive decline. *Sci Transl Med.* 2020;12(534):eaaz4069.
24. McKhann GM, Knopman DS, Chertkow H, et al. The diagnosis of dementia due to Alzheimer's disease: Recommendations from the National Institute on Aging–Alzheimer's Association workgroups on diagnostic guidelines for Alzheimer's disease. *Alzheimers Dement.* 2011;7(3):263–269.
25. Albert MS, DeKosky ST, Dickson D, et al. The diagnosis of mild cognitive impairment due to Alzheimer's disease: Recommendations from the National Institute on Aging–Alzheimer's Association workgroups on diagnostic guidelines for Alzheimer's disease. *Alzheimers Dement.* 2011;7(3):270–279.
26. Jack CR Jr, Bennett DA, Blennow K, et al. NIA-AA Research Framework: Toward a biological definition of Alzheimer's disease. *Alzheimers Dement.* 2018;14(4):535–562.
27. Gorno-Tempini ML, Brambati SM, Ginex V, et al. The logopenic/phonological variant of primary progressive aphasia. *Neurology.* 2008;71(16):1227–1234.
28. Mendez MF, Ghajarian M, Perryman KM. Posterior cortical atrophy: clinical characteristics and differences compared to Alzheimer's disease. *Dement Geriatr Cogn Disord.* 2002;14(1):33–40.
29. Pedley TA. Interictal epileptiform discharges: Discriminating characteristics and clinical correlations. *Am J EEG Technol.* 1980;20(3):101–119.
30. Pillai J, Sperling MR. Interictal EEG and the diagnosis of epilepsy. *Epilepsia.* 2006;47(Suppl 1):14–22.
31. Hinkley LB, Vinogradov S, Guggisberg AG, Fisher M, Findlay AM, Nagarajan SS. Clinical symptoms and alpha band resting-state functional connectivity imaging in patients with schizophrenia: Implications for novel approaches to treatment. *Biol Psychiatry.* 2011;70(12):1134–1142.
32. Nolte G, Bai O, Wheaton L, Mari Z, Vorbach S, Hallett M. Identifying true brain interaction from EEG data using the imaginary part of coherency. *Clin Neurophysiol.* 2004;115(10):2292–2307.
33. Dalal SS, Zumer JM, Guggisberg AG, et al. MEG/EEG source reconstruction, statistical evaluation, and visualization with NUTMEG. *Comput Intell Neurosci.* 2011;2011:758973.
34. Dalal SS, Guggisberg AG, Edwards E, et al. Five-dimensional neuroimaging: Localization of the time–frequency dynamics of cortical activity. *NeuroImage.* 2008;40(4):1686–1700.
35. Guggisberg AG, Honma SM, Findlay AM, et al. Mapping functional connectivity in patients with brain lesions. *Ann Neurol.* 2008;63(2):193–203.
36. Ranasinghe KG, Rankin KP, Lobach IV, et al. Cognition and neuropsychiatry in behavioral variant frontotemporal dementia by disease stage. *Neurology.* 2016;86(7):600–610.
37. Smailovic U, Koenig T, Kareholt I, et al. Quantitative EEG power and synchronization correlate with Alzheimer's disease CSF biomarkers. *Neurobiol Aging.* 2018;63:88–95.
38. Truccolo W, Donoghue JA, Hochberg LR, et al. Single-neuron dynamics in human focal epilepsy. *Nat Neurosci.* 2011;14(5):635–641.
39. Canuet L, Pusil S, Lopez ME, et al. Network disruption and cerebrospinal fluid amyloid-beta and phospho-tau levels in mild cognitive impairment. *J Neurosci.* 2015;35(28):10325–10330.
40. Nakamura A, Cuesta P, Fernandez A, et al. Electromagnetic signatures of the preclinical and prodromal stages of Alzheimer's disease. *Brain.* 2018;141(5):1470–1485.
41. Musaeus CS, Shafi MM, Santarnecchi E, Herman ST, Press DZ. Levetiracetam alters oscillatory connectivity in Alzheimer's disease. *J Alzheimers Dis.* 2017;58(4):1065–1076.
42. Vossel K, Ranasinghe K, Beagle AJ, et al. Effect of levetiracetam on cognition in patients with Alzheimer disease with and without epileptiform activity. *JAMA Neurol.* 2021;78(11):1345–1354.
43. Bakker A, Krauss GL, Albert MS, et al. Reduction of hippocampal hyperactivity improves cognition in amnesic mild cognitive impairment. *Neuron.* 2012;74(3):467–474.
44. Tong X, An D, Xiao F, et al. Real-time effects of interictal spikes on hippocampus and amygdala functional connectivity in unilateral temporal lobe epilepsy: An EEG–fMRI study. *Epilepsia.* 2019;60(2):246–254.
45. Lagarde S, Roehri N, Lambert I, et al. Interictal stereotactic-EEG functional connectivity in refractory focal epilepsies. *Brain.* 2018;141(10):2966–2980.
46. Englot DJ, Konrad PE, Morgan VL. Regional and global connectivity disturbances in focal epilepsy, related neurocognitive sequelae, and potential mechanistic underpinnings. *Epilepsia.* 2016;57(10):1546–1557.
47. Bettus G, Ranjeva JP, Wendling F, et al. Interictal functional connectivity of human epileptic networks assessed by intracerebral EEG and BOLD signal fluctuations. *PLoS One.* 2011;6(5):e20071.